Check for updates

Bioelectromagnetics

WILEY

BioEM

RESEARCH ARTICLE OPEN ACCESS

Dosimetric Electromagnetic Safety of People With Implants: A Neglected Population?

Lena Kranold[1,2] | Jingtian Xi[3] | Tolga Goren[3] | Niels Kuster[3,4]

[1]Harry Perkins Institute of Medical Research, Perth, Western Australia, Australia | [2]School of Engineering, University of Western Australia, Perth, Western Australia, Australia | [3]IT'IS Foundation, Zeughausstrasse 43, Zurich, Switzerland | [4]Department of Information Technology and Electrical Engineering, Swiss Federal Institute of Technology (ETH Zurich), Zurich, Switzerland

Correspondence: Lena Kranold (lena.kranold@uwa.edu.au)

Received: 20 November 2024 | **Revised:** 5 September 2025 | **Accepted:** 9 September 2025

Funding: The project (21NRM05 STASIS) has received funding from the European Partnership on Metrology, co-financed by the European Union's Horizon Europe Research and Innovation Program and by the Participating States.

Keywords: exposure assessment | implant safety | induced electric field | wireless power transfer

ABSTRACT

Electromagnetic (EM) safety guidelines are designed to protect the general public and workers from the risks posed by exposure to EM sources of all types, with the exception of medical EM sources. However, it has never been systematically evaluated whether individuals with conductive implants are also protected by these guidelines or whether the local field enhancement due to presence of the implant may pose an unacceptable risk under certain realistic exposure conditions. To address this important knowledge and regulatory gap, we first evaluated the upper bound of the local enhancement of bare and insulated generic implants of 0.5 λ (approximately equal to resonant) and 0.1 λ lengths, but restricted the maximum length to 2 m, as a function of tissue properties and frequency (10 kHz to 1 GHz). Results for uniform electric field excitation showed local enhancement of $psSAR_{10mg}$ and of locally averaged E-field, respectively, compared to the background in the presence of a generic implant of 10 dB (1 GHz) to over 100 dB at frequencies under 100 MHz. In the next step, we tested the hypothesis that fields induced inside the human body by realistic near-field sources are not sufficiently uniform to generate results in enhancement that could pose unacceptable risk. Common implant trajectories were inserted into the Virtual Population human anatomical model Ella V3.0, and the model was exposed to the following conditions (i) a standard source representing a wireless power transfer source operating at 85 kHz and (ii) a dipole source that operates at 450 MHz within the current exposure limits. Results show that the safety limit is exceeded at the tip of the implant by a factor of > 10 (> 20 dB) or > 115 V/m at 85 kHz, whereas the locally induced specific absorption rate averaged over 10 mg at 450 MHz was 7.9 W/kg, resulting in a temperature increase after 6 min of < 0.4 K. Hence, as the hypothesis was falsified at frequencies < 450 MHz, patients with implants are inadequately protected by current safety and product guidelines. In the discussions, proposals for how to close this regulatory gap are provided. Bioelectromagnetics. 00:00–00, 2025. © 2025 Bioelectromagnetics Society.

1 | Introduction

The use of strong electromagnetic (EM) sources, which can be operated in close proximity to the human body, open up major possibilities, as they provide enhanced functions of devices and conveniences for our daily lives. Examples include wireless communication systems such as smartphones, handheld computers, and the Internet of Things. EM exposure is expected to become even more ubiquitous in all of our activities. The replacement of wired charging systems with wireless power

This is an open access article under the terms of the Creative Commons Attribution-NonCommercial License, which permits use, distribution and reproduction in any medium, provided the original work is properly cited and is not used for commercial purposes.

© 2025 The Author(s). *Bioelectromagnetics* published by Wiley Periodicals LLC on behalf of Bioelectromagnetics Society.

Summary

- In this study, we evaluated systematically whether people with conductive implants are protected by electromagnetic safety guidelines and standards or whether certain exposure conditions result in an unacceptable risk to the subpopulation.
- A systematic exposure study of generic insulated and non-insulated implants showed local enhancements of the $psSAR_{10mg}$ and locally averaged E-field in a frequency range of 10 kHz to 1 GHz of up to 100 dB.
- The human anatomical model ViP Ella v3 with common implant trajectories was exposed to a realistic 85 kHz wireless power transfer coil and a 450 MHz dipole source, resulting in a local field enhancement at the implant tip of over >115 V/m and 7.9 W/kg, respectively, showing that people with implants are not adequately protected by current safety guidelines.

transfer (WPT), e.g., for mobile phones and electric vehicles (EV), is just beginning (Fortune Business Insights 2032).

Various organizations have developed EM safety guidelines, e.g., (International Commission on Nonionizing Radiation Protection ICNIRP 1998, 2010, 2020; IEEE 1992, 2006, 2019; Qualcomm Technologies Inc 2014) to protect people from the potential hazards of these EM exposures, e.g., vascular hazards due to whole-body specific absorption rate (SAR), thermal tissue damage by local absorption, and unintended nerve excitation by induced electric (E-)fields. Limits are defined for induced SAR from 100 kHz–10 GHz and induced E-field from 0 to 10 MHz.

In parallel with the increasing usage of wireless devices, the proportion of the population requiring passive or active medical implants is also growing. Historical trends and predictions for the next decade show that the number of people affected will grow into a significant sub-population, as the predicted growth rate of the market is 7.2% (Fairfield Market Research 2024). When the human body is exposed to EM radiation, the presence of an implant can significantly enhance the local E-field or SAR as the conductive implant becomes an antenna-like structure within the tissue environment. A severe accident suffered by a patient with a deep brain stimulator (DBS) implant exposed to a 1.0 T magnetic resonance imaging (MRI) scanner has been documented (Henderson et al. 2005); the accident resulted in neural dysfunctions and permanent neurological damage. In response, experts formed a technical committee and drafted a standardization document ISO10974 to guide and assess the safety of patients with active implants during MRI scans (ISO 2022). In addition, (ASTM 2023) serves as a guidance document for assessing the risks of people with passive implants in the MRI environment. It should be noted that the acceptable level of exposure to fields induced by MRI scanners is much higher than that allowed by the EM safety guidelines for the general population and workers.

None of the above listed safety guidelines and product standards for nonmedical devices address the potential hazards of local field enhancements by the presence of the implants. The language in articles B.2.2.5 and B.7.8 of (IEEE 2019) points simply to the risk of local field enhancement potentially caused by metallic implants but does not provide a mitigation strategy to assess the risks to this sub-population.

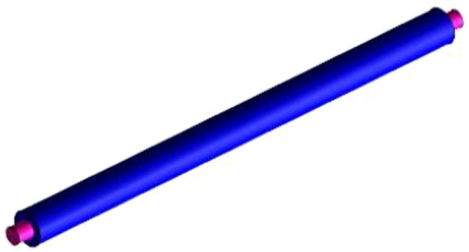


FIGURE 1 | Model of insulated implant (not to scale).

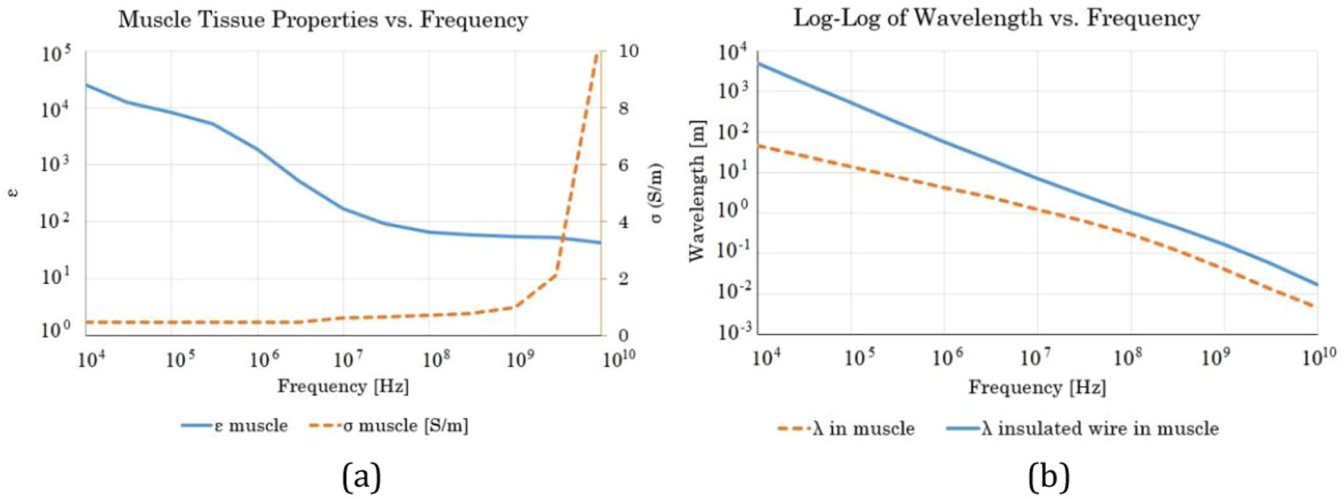


FIGURE 2 | (a) Muscle tissue dielectric properties and (b) wavelength in muscle and King wavelength of an insulated antenna as a function of frequency.

1521186x, 2025, 6, Downloaded from https://onlinelibrary.wiley.com/doi/10.1002/bem.70023, Wiley Online Library on [29/09/2025]. See the Terms and Conditions (https://onlinelibrary.wiley.com/terms-and-conditions) on Wiley Online Library for rules of use; OA articles are governed by the applicable Creative Commons License

Until today, only a relatively small number of studies have addressed the issue for general EM sources. King et al (King et al. 1974). analytically solved the EM problem of embedded insulated antennas as a function of dielectric tissue properties. Meier (Meier 1996) investigated the SAR enhancement of implants exposed to body-mounted antennas operating at 900 MHz in the context of compliance testing; they found a maximal local enhancement of the peak spatial SAR averaged over 1 g tissue cube (psSAR1g) in muscle of only a factor 4 compared to the background SAR. Kyriakou et al (Kyriakou et al. 2012). investigated the local enhanced psSAR in the presences of the generic implant proposed by the Food and Drug Administration (FDA) for different implant lengths exposed to different frequencies (10–1000 MHz) and found strong enhancement at low frequencies. The findings of Liorni et al (Liorni et al. 2018). complement those of (King et al. 1974) by generalizing the interaction of electrically short implants. The study showed that the local field enhancements for implants $< 0.2\,\lambda$ in ohmic contact with the tissue can be approximated by the current driven by the difference in voltage between the two endpoints in contact with the tissue. Additionally, Schmid et al (Schmid et al. 2024). investigated whether the exposure risk of workers with passive metallic implants in the wrist when the source is compliant with the EU directive of minimum health and safety (Official Journal of the European Union 2013) and found that the presence of the implant enhances locally induced EM fields, potentially resulting in unintended stimulation.

TABLE 1 | Wavelengths and respective implant lengths considered in this study.

frequency (Hz)	λ_{King} (m)	simulated length 0.1 λ (m)	simulated length 0.5 λ (m)
1×10^4	4827	2	2
3×10^4	1665	2	2
1×10^5	519	2	2
3×10^5	180	2	2
1×10^6	56.4	2	2
3×10^6	19.7	1.97	2
1×10^7	6.25	0.625	2
3×10^7	2.21	0.221	1.11
1×10^8	0.716	0.0716	0.385
3×10^8	0.267	0.0267	0.134
1×10^9	0.0994	0.00994	0.0497

To generalize the above findings for any conductive implant, we investigated the exposure scenarios in which persons with passive or active implants may be subject to a potential risk due to field enhancements when exposed to real-world EM sources that are compliant according to today's regulations and discuss potential mitigation strategies. We do not address the additional risk of malfunctions due to EM interference of active implants.

2 | Methods

In this study, we extend previous studies (King et al. 1974; Meier 1996; Kyriakou et al. 2012; Liorni et al. 2018) by systematically investigating the local enhancement caused by the presence of partially isolated and non-isolated implants in different tissues for the entire range of lengths and test whether these enhancements also occur for typical implants

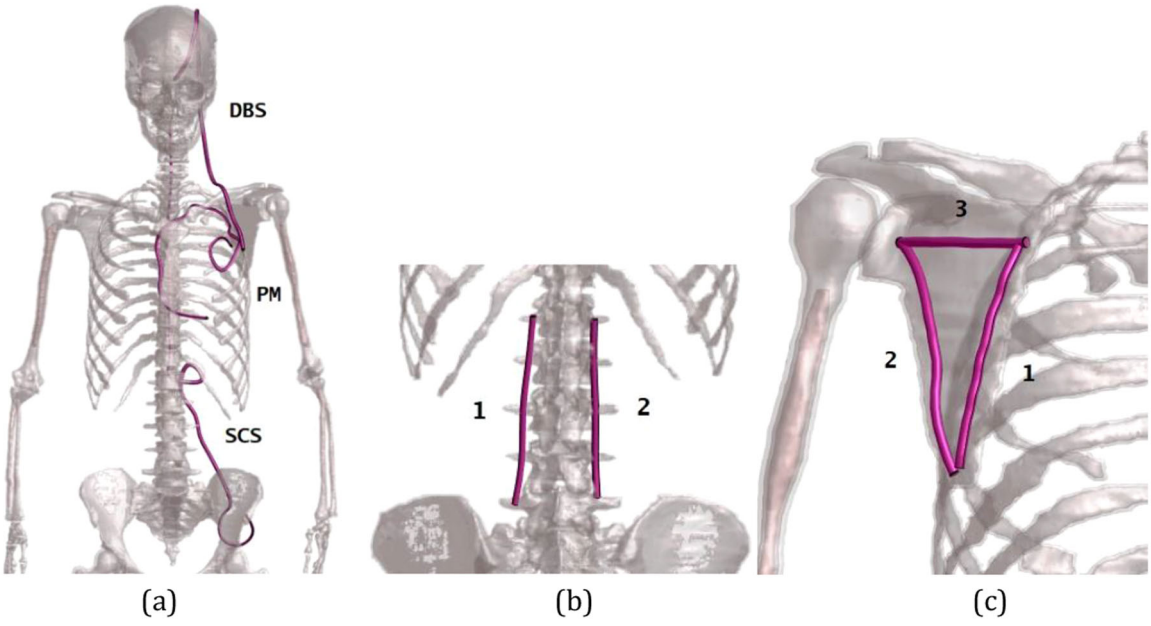


FIGURE 3 | Selected splines simulated in the human anatomical ViP model Ella V3.0: (a) DBS, PM, and SCS splines, (b) lumbar splines L1 and L2, and (c) shoulder splines S1, S2, and S3.

1521186x, 2025, 6, Downloaded from https://onlinelibrary.wiley.com/doi/10.1002/bem.70023, Wiley Online Library on [29/09/2025]. See the Terms and Conditions (https://onlinelibrary.wiley.com/terms-and-conditions) on Wiley Online Library for rules of use; OA articles are governed by the applicable Creative Commons License

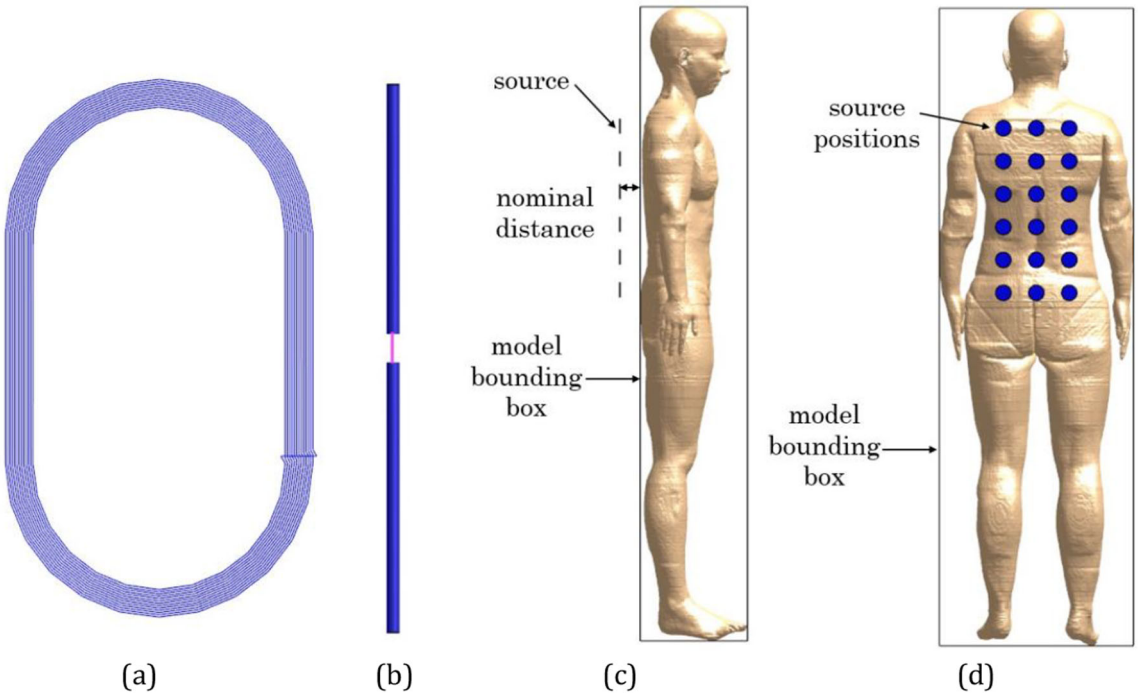


FIGURE 4 | Safety simulation performed with the human anatomical ViP model Ella V3.0: (a) 85 kHz coil source, (b) 450 MHz dipole source (dimensions not to scale), (c) side view, and (d) back view of the source positions and bounding box in proximity to Ella V3.0. were extracted. At 85 kHz, the induced E-field along the splines was extracted and integrated over the implant spline length to determine the voltage difference between the two endpoints (Liorni et al. 2018). At 450 MHz, the average of the tangential E-fields, which is a good metric for the deposited power (ISO 2022), was computed. A summary of the spline lengths as a function of λ is given in Table 2.

TABLE 2 | Implant spline lengths expressed in terms of wavelength in muscle.

	DBS	PM	SCS	L1	L2	S1	S2	S3
85 kHz	0.016λ	0.003λ	0.004λ	0.013λ	0.022λ	0.002λ	0.003λ	0.002λ
450 MHz	6.8λ	1.4λ	1.5λ	5.7λ	9.6λ	0.8λ	1.3λ	1.0λ

implanted in anatomical models exposed to realistic sources. The sources are driven at the maximum permissible power meeting the relevant basic restrictions according to IC-NIRP2010. All simulations were conducted in Sim4Life v7.0 and v8.0 (ZMT Zurich MedTech AG 2025). For frequencies > 3 MHz, the EM finite-differences time-domain (FDTD) solver was used, and, for lower frequencies, a quasistatic approximation with the electroquasistatic (EQS) and magneto-quasistatic (MQS) solver was applied (Hirata et al. 2013; Park et al. 2013; Laakso 2020). The enhancements with compared to without implants were assessed of the hazard-relevant quantities, i.e., $psSAR_{10g}$ for external sources, $psSAR_{10mg}$, the maximal electrical E-field average of a cube of 2.15 mm side length, $E_{rms,\ max,2.15\times2.15\times2.15,}$ (same as $psSAR_{10mg}$ in dB for homogeneous tissues) and over a cube of 2 mm side length, $E_{rms,\ max,2\times2\times2.}$ The maximum values are reported instead of the 99th percentile, as the discretization is always better than 1 mm, thereby strongly limiting potential artifacts. The 99th percentile is also strongly underestimating the exposures for very localized sources (De Santis et al. 2012).

2.1 | Generic Implant Exposed to Frequencies of 10 KHz–1 GHz

The enhancement caused by a simplified implant model over the background was investigated at different frequencies. Implants of two lengths expressed in terms of wavelength were investigated a short ($l = \lambda/10$) implant and an approximately resonant ($l = \lambda/2$) generic implant. The insulated implants are based on the SAIMD-U (ZMT Zurich MedTech AG 2025); the passive implants consist of the same wire without insulation. Examples for active, insulated implants include pacemakers or neurostimulators, and passive implants include bone fixtures and screws. However, the maximal length was restricted to 2 m as the lengths of realistic implants reported to be up to 1.61 m (Henderson et al. 2005). The implants were excited with a constant E-field tangential to their lengths, in the form of parallel plates for frequencies < 10 MHz and plane waves for frequencies ≥ 10 MHz. The investigation was performed in tissues representing muscle and fat, as well as two tissues, denoted as Tissues A and B, having relative permittivity and conductivity properties averaged between those of muscle and

1521186x, 2025, 6, Downloaded from https://onlinelibrary.wiley.com/doi/10.1002/bem.70023, Wiley Online Library on [29/09/2025]. See the Terms and Conditions (https://onlinelibrary.wiley.com/terms-and-conditions) on Wiley Online Library for rules of use; OA articles are governed by the applicable Creative Commons License

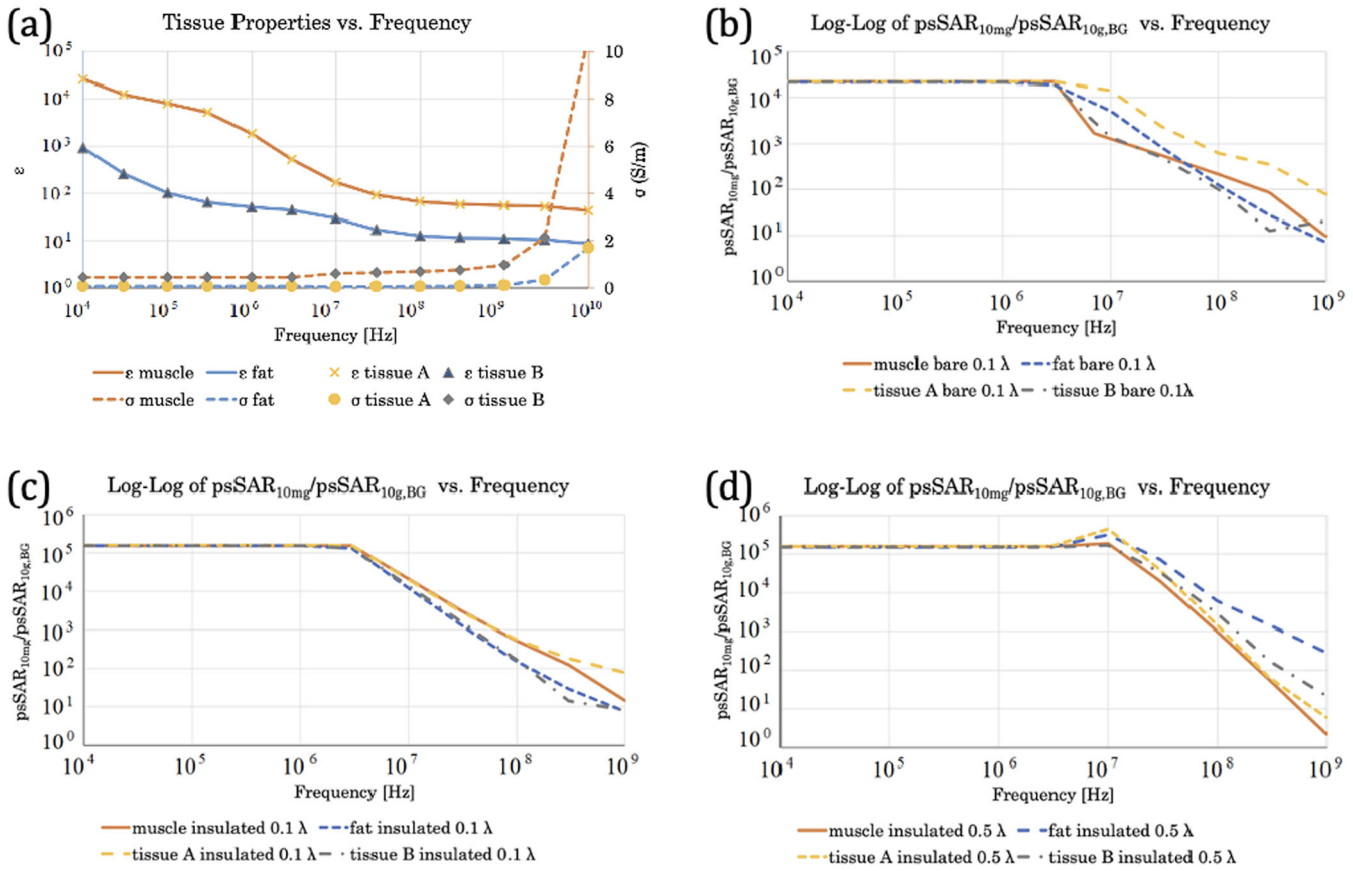


FIGURE 5 | Ratio of the enhanced $psSAR_{10mg}$ of simplified implants over background $psSAR_{10g}$ as a function of frequency across the range 10^4–10^9 Hz in four tissues: muscle (orange), fat (blue), tissue A (yellow), and tissue B (gray); (a) dielectric properties of muscle and fat tissues ε_r (solid line) and σ (dashed line), with data for tissues A and B superimposed as markers; (b) enhancement of ratio of the bare implant of length 0.1 λ; (c) enhancement ratio of the insulated implant of length 0.1 λ; and (d) enhancement ratio of the insulated implant of length 0.5 λ.

fat tissue (Hasgall et al. 2025). Tissue A represents a high permittivity and low conductivity tissue and Tissue B a low permittivity and high conductivity tissue, ranging across permittivity and conductivity range of muscle and fat. The enhancement is evaluated as the ratio of local enhancement $psSAR_{10mg}$ over background $psSAR_{10g}$.

The insulated generic implant has a conductor diameter of 1 mm and an insulator thickness of 1 mm. Both tips of the conductor are exposed at a length of 1 mm. The conductor was modeled as a perfect electric conductor (PEC) with insulation dielectric properties of $\varepsilon_r = 3$ and $\sigma = 0$ S/m. The corresponding passive implant is a PEC wire of the same dimensions as the conductor of the insulated generic implant. Figure 1 shows an example of the generic implant.

The frequencies investigated ranged from 10 kHz to 1 GHz. Figure 2 shows the dielectric properties (a) of muscle tissue (Hasgall et al. 2025) and the King wavelength, which has been calculated following the process described in (King et al. 1969) of insulated antennas compared to the wavelength (b) in muscle tissue over the frequency range of interest. For this investigation, the antenna wavelength serves as the reference to determine the implant length. Table 1 summarizes the frequencies under consideration and the corresponding implant lengths used in the simulation.

2.2 | Generic Implants in a Human Anatomical Model

We also set out to validate the hypothesis that the fields induced in the complex and nonhomogeneous anatomical tissue composition of the human body along actual implant trajectories by realistic sources are insufficient to give rise to any relevant local field enhancement that could pose a risk to patients. To test our hypothesis, common active implants, including a DBS, a pacemaker (PM), a spinal cord stimulator (SCS), and passive lumbar and shoulder implants were modeled inside the human anatomical model Ella V3.0 of the Virtual Population (ViP) (Gosselin et al. 2014) (see Figure 3). Ella was exposed to two different realistic validation sources: a 85 kHz WPT source and a 450 MHz dipole source. Ella—a female full human anatomical model, 26 years old, 1.63 m tall with a body-mass index of 21.6 kg/m^2—is derived from high-resolution MRI scans in which 305 different tissues are segmented. The most commonly used implant trajectories were defined in the ViP model Ella V3.0. The E-fields induced by

1521186x, 2025, 6, Downloaded from https://onlinelibrary.wiley.com/doi/10.1002/bem.70023, Wiley Online Library on [29/09/2025]. See the Terms and Conditions (https://onlinelibrary.wiley.com/terms-and-conditions) on Wiley Online Library for rules of use; OA articles are governed by the applicable Creative Commons License

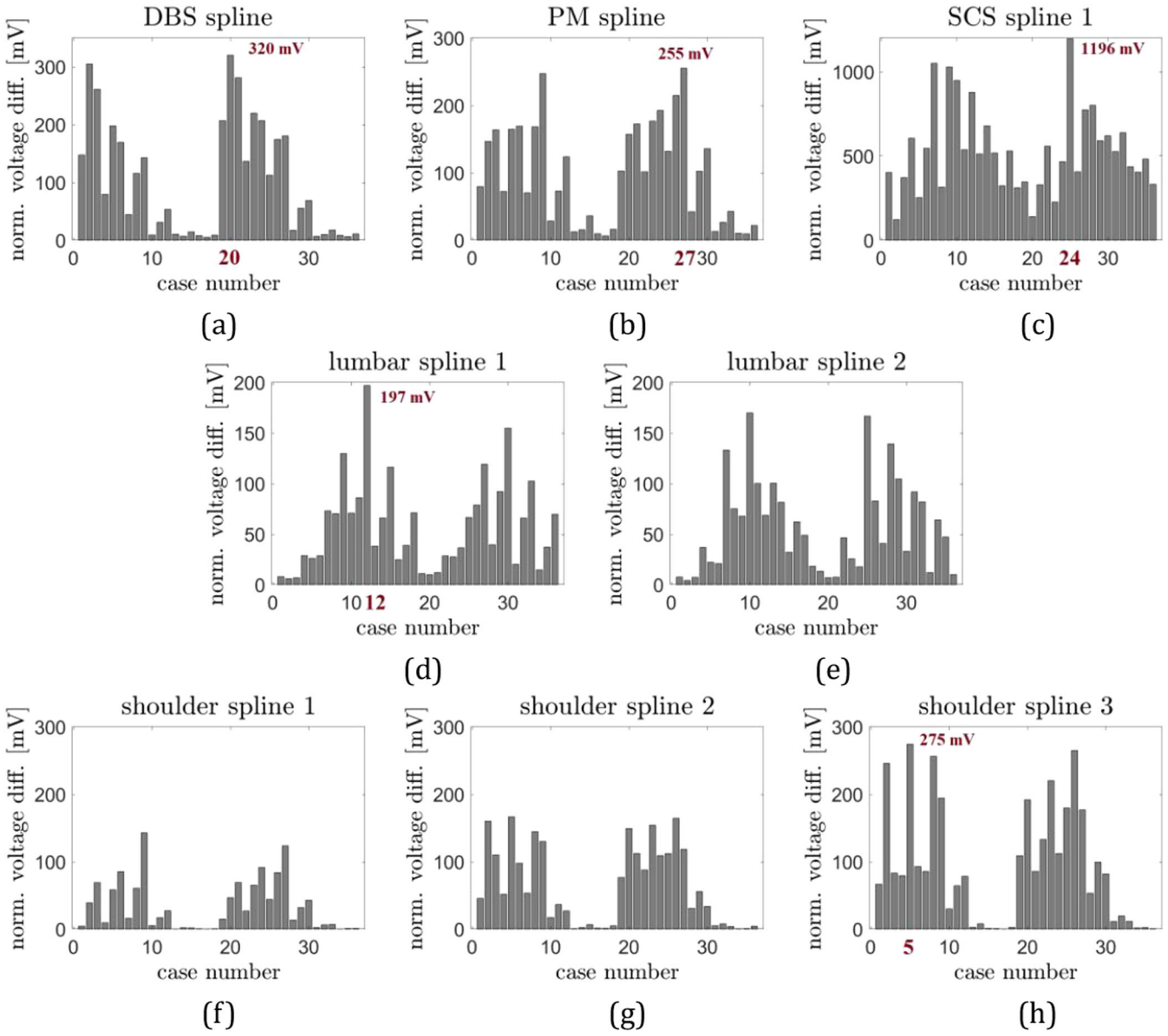


FIGURE 6 | Induced voltage histograms of selected splines exposed to the 85 kHz source; the case numbers refer to the positions on Ella's back (see Figure 4(d)), starting at case1 for the top left to case 18 at the bottom right for the source positioned at a distance of 2 mm, and cases 19–36 for the source at 50 mm distance; case numbers corresponding to the highest induced voltages for each spline type are labeled red: (a) DBS, (b) PM, (c) SCS, (d) L1, (e) L2, (f) S1, (g) S2, and (h) S3.

the validation sources along these trajectories were determined to derive conservative exposure scenarios. A single trajectory was chosen for each of the active implants (DBS, PM, SCS). The lumbar implant had two independent splines (L1 and L2), one on each side of the spine, and three independent shoulder implant trajectories (S1, S2, and S3). The implant trajectories are displayed in Figure 3. The implants are electrically short at 85 kHz (0.002–0.022 λ) and electrically long at 450 MHz (1.0–9.6 λ).

A small generic 85 kHz WPT coil with 13 turns was modeled as an elliptically shaped wire coil with outer axes diameters of 350 mm by 200 mm and inner axes diameters of 314 mm by 164 mm, (SPEAG 2025). The second realistic source, chosen according to the validation sources described in (IEC/IEEE 2025, 2020), was modeled as a 450 MHz resonant dipole with length of 290 mm and overall height of 330 mm. The chosen sources are compliant with (IEC/IEEE 2025, 2020; IEC PAS 2025) as a validation and verification source for system performance testing before measuring an unknown source. In total, 36 cases of source placements, based on (IEC/IEEE 2020), were assessed in a 3×6 grid on the back of the ViP model, at distances of 2 mm and 50 mm from the model bounding box.

The resolution of these simulations was set to 0.625 mm in proximity to the implant, 2 mm outside the region of interest for the WPT source, and 1 mm for the dipole source. Figure 4 shows (a) the coil model, (b) the dipole source, (c) the bounding box and ViP model Ella V3.0, and (d) the source positions.

1521186x, 2025, 6, Downloaded from https://onlinelibrary.wiley.com/doi/10.1002/bem.70023, Wiley Online Library on [29/09/2025]. See the Terms and Conditions (https://onlinelibrary.wiley.com/terms-and-conditions) on Wiley Online Library for rules of use; OA articles are governed by the applicable Creative Commons License

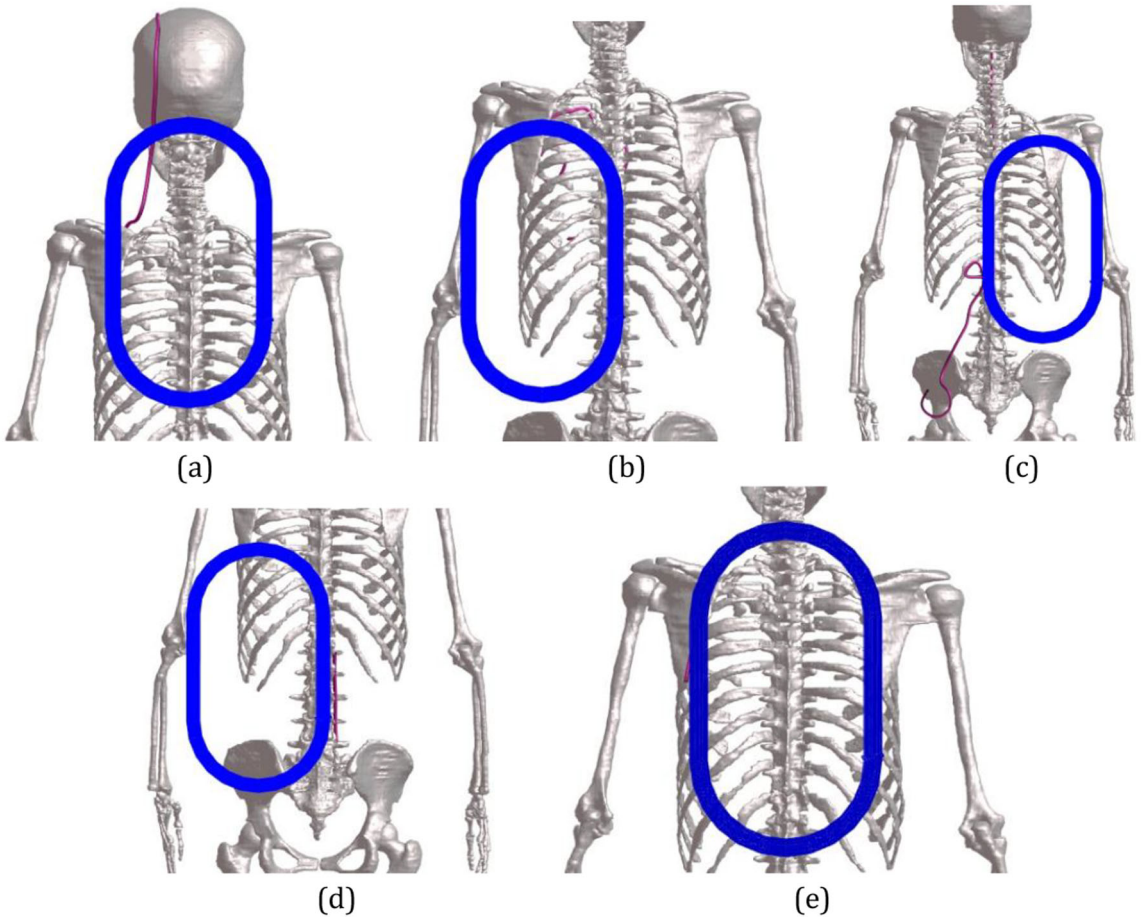


FIGURE 7 | Implant positions resulting in maximum exposures to the 85 kHz source positions for the (a) DBS, (b) PM, (c) SCS, (d) L1, and (e) S3 implants.

To assess conservative scenarios, the ViP model without implants was exposed to the 36 different source positions, and the E-fields induced along the implant trajectories were extracted.

For the conservative source placement of each routing and source type, an actual implant was placed inside the ViP model Ella V3.0.

In the case of the 85 kHz WPT source, the peak E-field as well as the restrictive quantity according to (International Commission on Nonionizing Radiation Protection ICNIRP 2010), the maximum cube-averaged rms E-field over cubes of 2 mm lengths, $E_{rms,\ max,2\times2\times2}$, was extracted in agreement with ICNIRP guidelines (International Commission on Nonionizing Radiation Protection ICNIRP 1998, 2010, 2020), and both results were scaled to the input power of the coil positioned to lead to the maximum induced E-field of 11.5 V/m, in the case of ViP Ella V3.0, with no implant present. The result was then evaluated to assess whether the coil operates within safety limits in the presence of an implant.

In the case of the 450 MHz dipole source, the $psSAR_{10mg}$ was extracted as the restrictive quantity at that frequency according to (International Commission on Nonionizing Radiation Protection ICNIRP 1998; IEEE 2019). $psSAR_{10mg}$—much better proxy of temperature increase for localized sources—was selected instead of $psSAR_{10g}$. The results in both cases, with and without implant, where scaled to the input power at the dipole source that leads to the maximum deposited $psSAR_{10g}$ of 2 W/kg in the case of ViP model Ella V3.0 with no implant present. The result was then evaluated to assess whether the dipole operates within safety limits in the presence of an implant.

The active DBS, PM, and SCS implants were modeled as conductors of diameter of 1 mm and insulator thickness of 1 mm, and both ends were simplified as exposed ends of splines of 1 mm length. The total length corresponds to the length of the spline listed in Table 2. The dielectric properties of the conductor and insulator were the same as stated in Section 2.1, $\varepsilon_r = 3$ and $\sigma = 0$ S/m. The passive lumbar and shoulder implants were modeled as PECs of thickness 2 mm.

3 | Results

3.1 | Generic Implant Exposed to Frequencies of 10 kHz–1 GHz

The local enhancement in $psSAR_{10mg}$, normalized to background enhancement of $psSAR_{10g}$ under the same conditions, is displayed in Figure 5.

1521186x, 2025, 6, Downloaded from https://onlinelibrary.wiley.com/doi/10.1002/bem.70023, Wiley Online Library on [29/09/2025]. See the Terms and Conditions (https://onlinelibrary.wiley.com/terms-and-conditions) on Wiley Online Library for rules of use; OA articles are governed by the applicable Creative Commons License

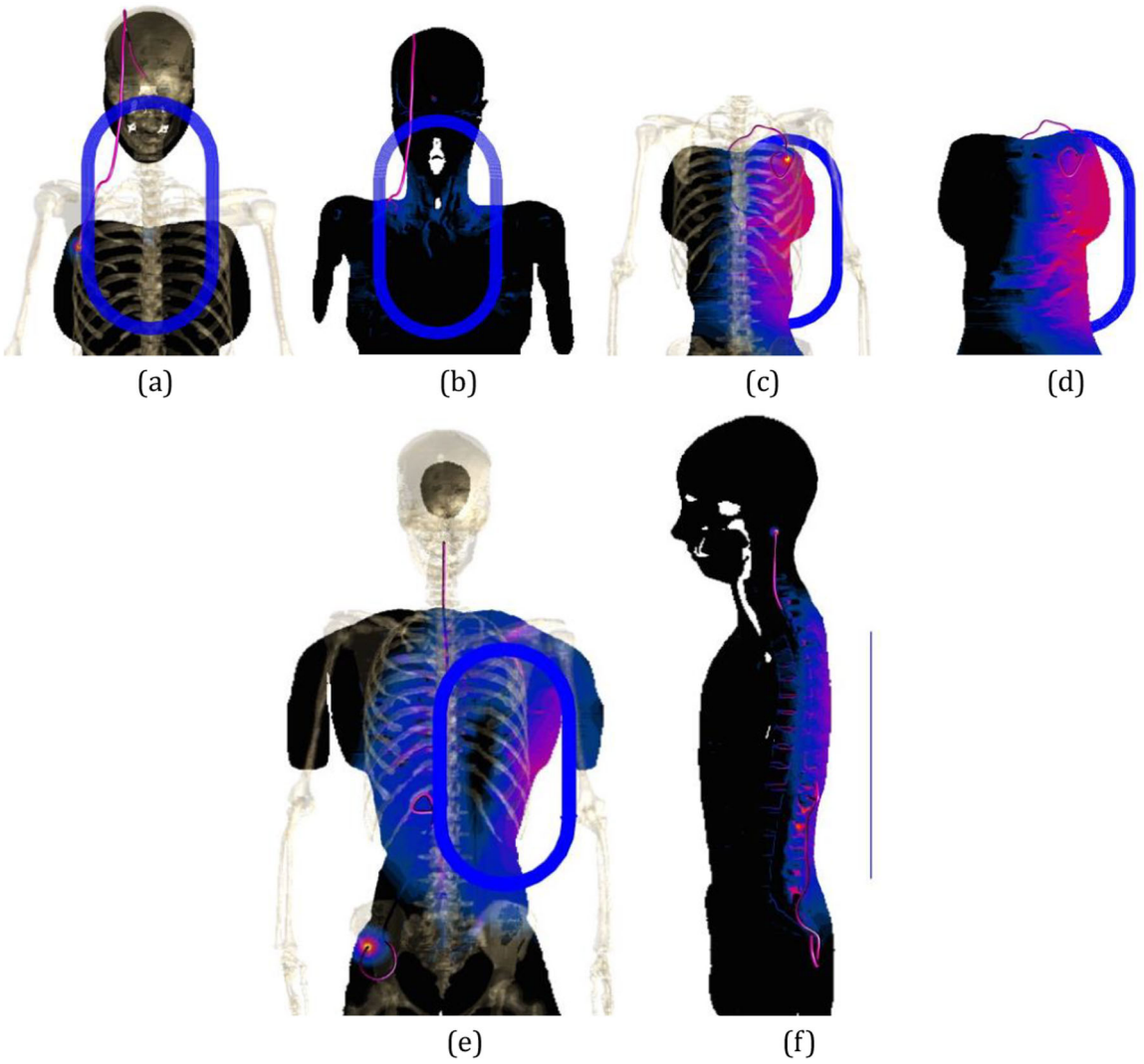


FIGURE 8 | Cross-sectional slices of the maximum field distributions of active implants exposed to the 85 kHz source: (a) *xy*-slice of the DBS IPG end, (b) *xy*-slice of the DBS electrode end, (c) *xy*-slice of the PM IPG end, (d) *xy*-slice of the PM electrode end, (e) *xy*-slice of the SCS IPG end, and (f) *xz*-slice of the SCS electrode end.

It can be observed that even the electrically short implant leads ($\leq 0.2\,\lambda$), displayed in Figure 5 (b) and (c), exhibit local enhancement in psSAR_{10mg} and $E_{\mathrm{rms,\ max,2.15\times2.15\times2.15}}$, respectively over the background of up to 60 dB at frequencies <70 MHz and of approximately 10 dB at 1 GHz. Due to the restriction that modeling implants cannot be longer than 2 m, the enhancement at frequencies <1 MHz is constant.

3.2 | Generic Implants in a Human Anatomical Model at 85 KHz

To determine the maximum exposure to the WPT coil, the voltage difference between the two ends of each trajectory for every exposure position was determined and is summarized in the histograms in Figure 6. The end-to-end voltages of the DBS routing are shown in (a), where exposure case 20 corresponds to the highest induced voltage of 320 mV. For the PM implant (b), case 27 corresponds to the highest induced voltage of 255 mV, and for the SCS spline (c), the highest induced voltage of 1196 mV is found in case 24. For the implants in the lumbar region, the right-sided implant site L1 (d) results in a maximum induced voltage of 197 mV (case 12), and maximum enhancement exhibited by the top shoulder spline S3 (h) is 275 mV (case 5). The source positioning for these five conditions of maximum exposure on which full-model simulations were performed are displayed in Figure 7.

In Figure 8, the field distributions at the electrode and the implantable pulse generator (IPG) ends of the active implants are shown, partially overlaid with the bone structure of ViP model Ella V3.0. Figure 9 shows the field distributions of the passive implants. The field distributions in all of these cases exhibit local field enhancements.

According to (International Commission on Nonionizing Radiation Protection ICNIRP 2010), the field quantity of interest for exposure at 85 kHz is the maximum cube-averaged rms E-field over a cube of 2 mm ($E_{\mathrm{rms,\ max,2\times2\times2}}$). When the coil is normalized to an input power corresponding to the maximum

1521186x, 2025, 6, Downloaded from https://onlinelibrary.wiley.com/doi/10.1002/bem.70023, Wiley Online Library on [29/09/2025]. See the Terms and Conditions (https://onlinelibrary.wiley.com/terms-and-conditions) on Wiley Online Library for rules of use; OA articles are governed by the applicable Creative Commons License

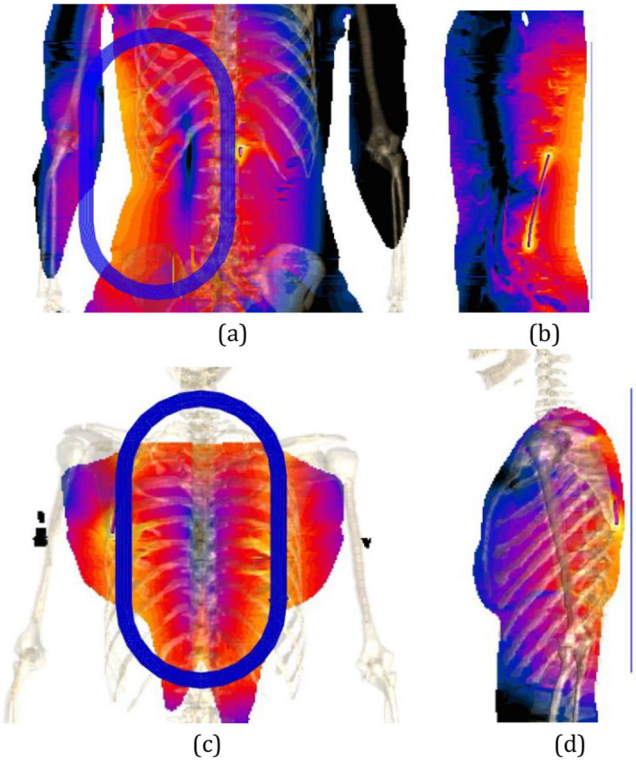


FIGURE 9 | Cross-sectional slices of the maximum field distributions of passive implants exposed to the 85 kHz source: (a) *xy*-slice of L1, (b) *xz*-slice of L1, (c) *xy*-slice of S3, and (d) *xz*-slice of S3.

TABLE 3 | Local enhancement of $E_{\text{rms, max,2×2×2}}$ due to the presence of an implant, normalized to a 85 kHz coil driven at the maximum E-field according to (International Commission on Nonionizing Radiation Protection ICNIRP 2010), for worst-case coil positions resulting as indicated in Figures 6 and 7..

Setup	$E_{\text{rms, max,2×2×2}}$ (V/m)	Enhancement (dB)
No implant	11.5	—
DBS	56	13.8
PM	20	4.7
SCS	122	20.5
L1	21	5.3
S3	33	9.2

permissible power transfer, the result in Ella in the absence of an implant is E = 11.5 V/m. The enhancement in $E_{\text{rms, max,2×2×2}}$ for each implant case is summarized in Table 3. In all cases, the limit of 11.5 V/m is exceeded by 4.7–20.5 dB.

The local peak E-field can exceed these limits even further. In Table 4, the peak E-field for each maximum coil position with and without the implant present, normalized to a coil power corresponding to the maximum $E_{\text{rms, max,2×2×2}} = 11.5$ V/m with no implant present, is summarized and the enhancement is calculated. The enhancement of the local peak E-field is between 3.3 and 18.3 dB, and in all cases, the limits according to (International Commission on Nonionizing Radiation Protection ICNIRP 2010) are well exceeded.

3.3 | Generic Implants in a Human Anatomical Model at 450 MHz

The maximum dipole exposure case at 450 MHz was determined by extracting the tangential E-field along the implant trajectories when the ViP model Ella V3.0 (Gosselin et al. 2014) is exposed to the dipole source. The average tangential E-fields along the spline for all of the 36 exposure scenarios are summarized in the histograms in Figure 10. The highest level of exposure to the dipole observed for the DBS, PM, and S3 implant routings, resulting on average tangential E-fields of 0.30, 0.20, and 2.9 V/m, respectively, were found for case 18. The maximal exposure of the SCS spline was found for case 30, with a tangential E-field of 0.86 V/m; maximum exposure of the L1 spline by the dipole was observed in case number 20, with an average tangential E-field of 1.2 V/m. Figure 11 shows the positions of the maximum exposure cases and the corresponding implant trajectories juxtaposed on the skeleton of the Ella model.

In Figure 12, the field distributions at the electrode and IPG ends of the active implants are shown, partially overlaid on the bone structure of the Ella model, and Figure 13 shows the field distributions of the passive implants.

Local field enhancements of the field distributions are observed in all of these cases. According to (International Commission on Nonionizing Radiation Protection ICNIRP 2020), the field quantity of interest for a 450 MHz

TABLE 4 | Local enhancement of peak E-field due to presence of the implant, normalized to the 85 kHz coil driven at maximum E-field according to (International Commission on Nonionizing Radiation Protection ICNIRP 2010), i.e., $E_{\text{rms, max,2×2×2}} = 11.5$ V/m.

Setup	$E_{peak,w/o\ implant}\left[\frac{V}{m}\right]$	$E_{peak,w\ implant}\left[\frac{V}{m}\right]$	Enhancement (dB)
DBS	24	140	15.3
PM	24	37	3.7
SCS	28	231	18.3
L1	23	38	4.3
S3	24	35	3.3

1521186x, 2025, 6, Downloaded from https://onlinelibrary.wiley.com/doi/10.1002/bem.70023, Wiley Online Library on [29/09/2025]. See the Terms and Conditions (https://onlinelibrary.wiley.com/terms-and-conditions) on Wiley Online Library for rules of use; OA articles are governed by the applicable Creative Commons License

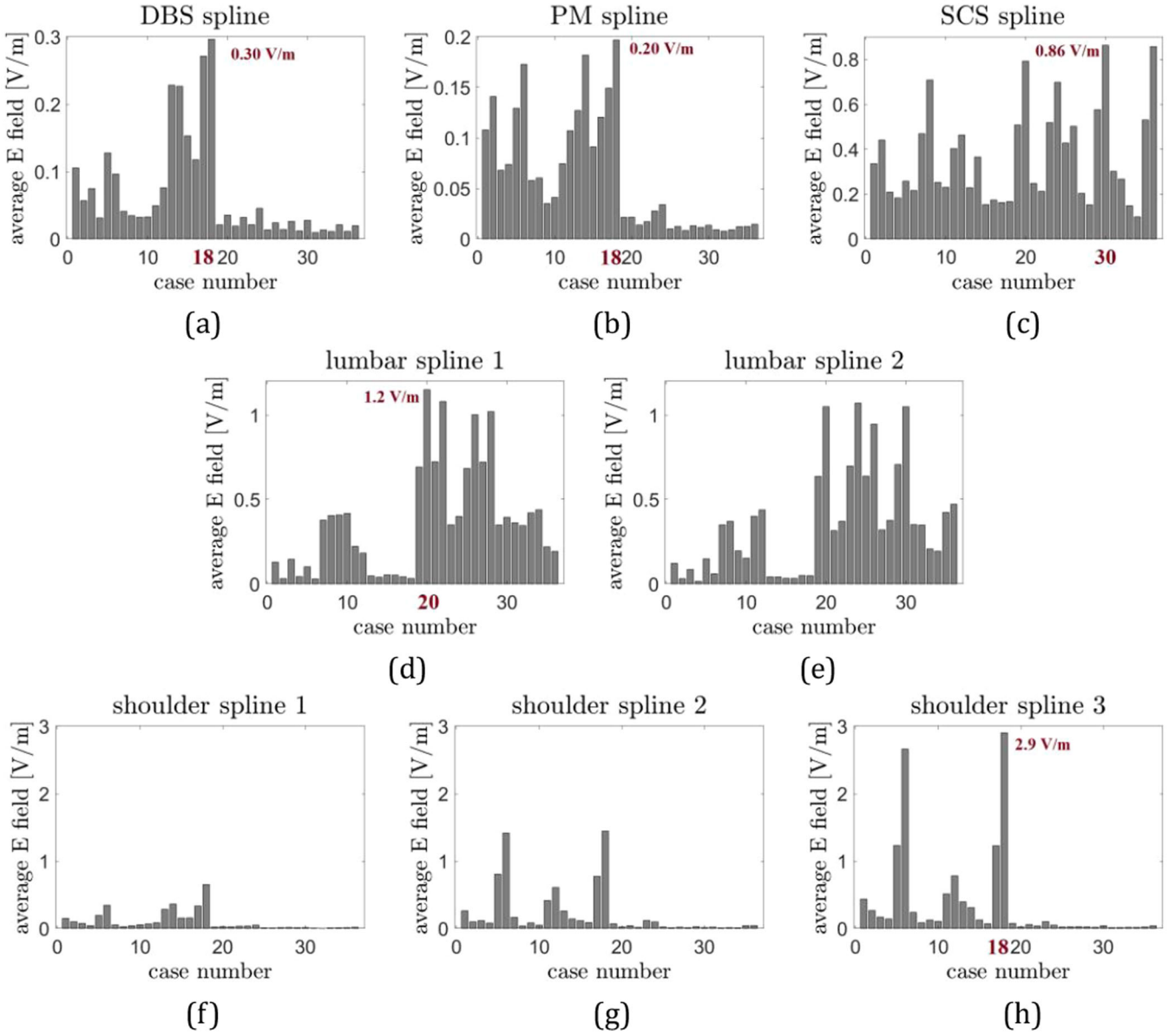


FIGURE 10 | Histograms showing the average tangential E-fields along selected splines exposed to 450 MHz source; the case numbers refer to the positions on Ella's back (see Figure 4(d)), starting at case1 for the top left to case 18 at the bottom right for the source positioned at a distance of 2 mm, and cases 19–36 for the source at 50 mm distance; case numbers corresponding to the highest induced voltages for each spline type are labeled red: (a) DBS, (b) PM, (c) SCS, (d) L1, (e) L2, (f) S1, (g) S2, (h) S3.

exposure is the localpsSAR. The general public exposure limit of psSAR10g = 2 W/kg in Ella with no implant present is reached when the dipole source is normalized to an input power that results in the maximum permissible power transmission; the enhancement of the psSAR10mg for each implant case investigated under these conditions is summarized in Table 5. The maximum very local psSAR10mg for the dipole operating at psSAR10g of 2–7.88 W/kg—found in the case of the SCS—corresponds to a local heating ΔT of approximately 0.35 K after 6 min of exposure, indicating that the increased risk posed to persons with medical implants is present only for local strong sources operating at frequencies < 450 MHz, with the only exception being the radiofrequency coils of MRI scanners.

4 | Discussion and Conclusions

In this study, we investigated the local maximum field levels experienced by patients with implants when exposed to sources compliant with current regulations within the frequency range of 10 kHz to 1 GHz. The enhancement of exposure was systematically analyzed for implants of realistic lengths that were subjected to uniform fields at the safety limits for induced fields (International Commission on Nonionizing Radiation Protection ICNIRP 1998, 2010, 2020; IEEE 2019). Our findings confirm the results of previous, more limited studies. Under uniform electric field excitation in homogeneous tissue equivalents, the local enhancement of psSAR10mg and the locally averaged E-field can exceed 10 dB at 1 GHz and reach

1521186x, 2025, 6, Downloaded from https://onlinelibrary.wiley.com/doi/10.1002/bem.70023, Wiley Online Library on [29/09/2025]. See the Terms and Conditions (https://onlinelibrary.wiley.com/terms-and-conditions) on Wiley Online Library for rules of use; OA articles are governed by the applicable Creative Commons License

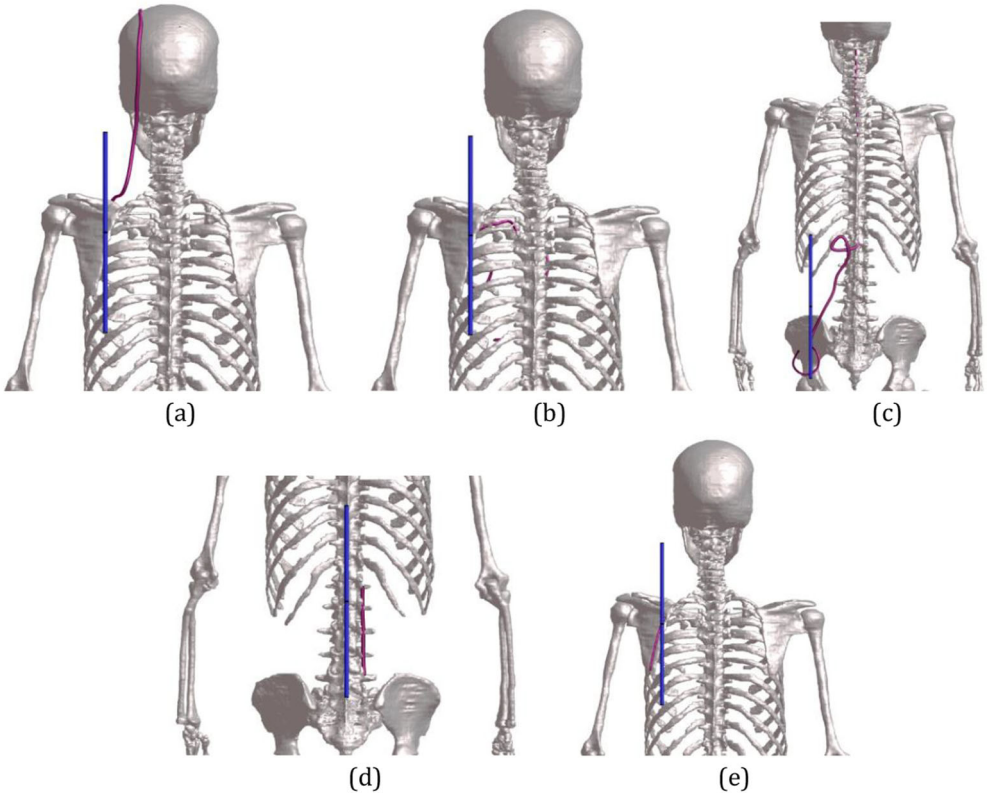


FIGURE 11 | Implant positions resulting in maximum exposures to the 450 MHz source for the (a) DBS, (b) PM, (c) SCS, (d) L1, and (e) S3 implants.

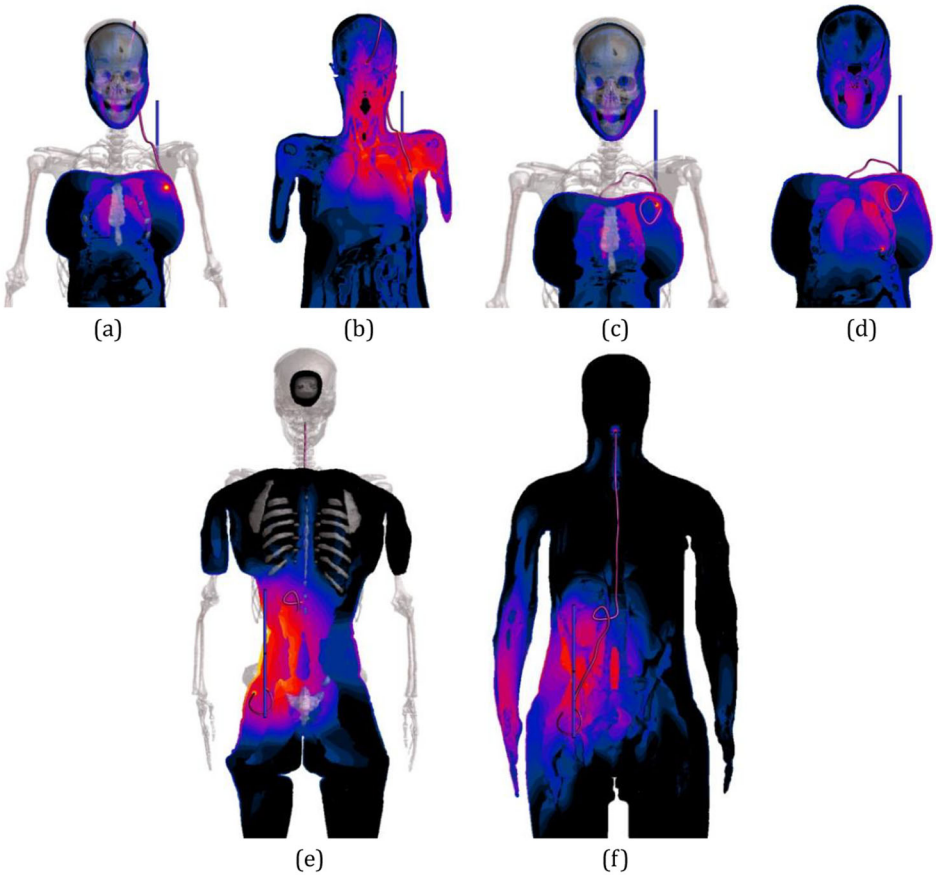


FIGURE 12 | Cross-sectional slices of the maximum field distributions of active implants exposed to the 450 MHz source: (a) *xy*-slice of the DBS IPG end, (b) *xy*-slice of the DBS electrode end, (c) *xy*-slice of the PM IPG end, (d) *xy*-slice of the PM electrode end, (e) *xy*-slice of the SCS IPG end, and (f) *xy*-slice of the SCS electrode end.

1521186x, 2025, 6, Downloaded from https://onlinelibrary.wiley.com/doi/10.1002/bem.70023, Wiley Online Library on [29/09/2025]. See the Terms and Conditions (https://onlinelibrary.wiley.com/terms-and-conditions) on Wiley Online Library for rules of use; OA articles are governed by the applicable Creative Commons License

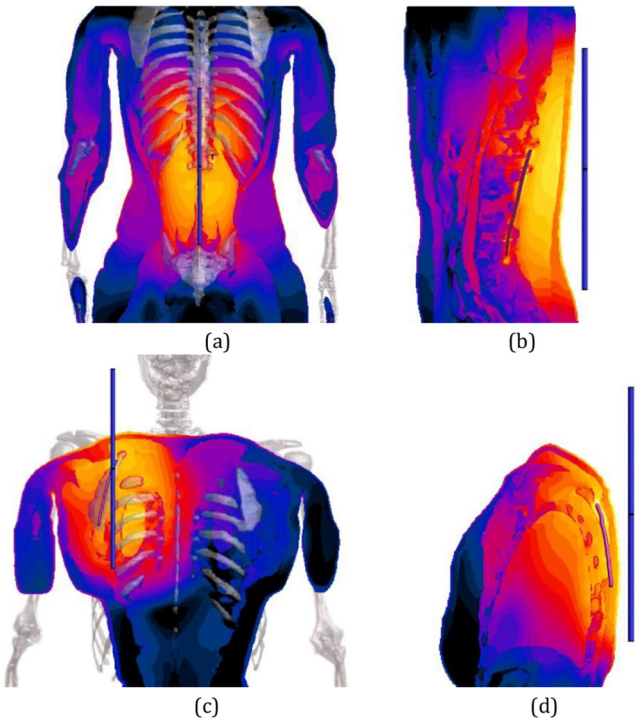


FIGURE 13 | Cross-sectional slices of the maximum field distributions of passive implants exposed to the 450 MHz source: (a) *xy*-slice of L1, (b) *xz*-slice of L1, (c) *xy*-slice of S3, and (d) *xz*-slice of S3.

TABLE 5 | Local enhancement of $psSAR_{10mg}$ due to the presence of the implant, normalized to a 450 MHz dipole driven at maximum $psSAR_{10mg}$ according to (International Commission on Nonionizing Radiation Protection ICNIRP 2020). Even though the enhancement is 13.2 dB, the temperature increase is <0.4 K.

Setup	psSAR10mg (W/kg)	Local enhancement (dB)	ΔT6min (K)
No implant	$psSAR_{10g} = 2$	—	—
DBS	1.97	5.0	<0.1
PM	2.00	3.3	<0.1
SCS	7.88	13.2	0.35
L1	2.38	4.5	<0.1
S3	6.41	9.9	<0.1

over 100 dB at frequencies below 100 MHz, compared to the background, in the presence of a generic implant. However, these findings are of limited practical value, as the fields induced inside a complex nonhomogeneous body by near-field sources are generally highly nonuniform. Hence, the realistic maximum enhancement is expected to be much smaller.

To address this, we tested the hypothesis that these enhancements might not be relevant for realistic implants and sources and pose no additional risk for patients with implants. However, we found for realistic trajectories and magnetic field sources operating at the limits for the general population, the local enhancements when compared to exposures without implants can be as large as 18.3 dB. In other words, these results of this study falsify this null-hypothesis, i.e., the enhancements are relevant for realistic scenarios. At 450 MHz, the dipole exposure increased the local SAR at the implant but the associated temperature increase was less than 0.4°C.

Some may argue that the current safety guidelines (International Commission on Nonionizing Radiation Protection ICNIRP 1998, 2010, 2020; IEEE 2019) include safety margins. However, these safety factors are designed to account for scientific uncertainty and inter-subject variability and are not designed to account for the presence of implants. Furthermore, the local enhancements were larger than the safety factors. Such enhancements are of particular concern in the context of life-supporting neurostimulators.

This study reports only the relative enhancements; therefore, uncertainties affecting the absolute results—such as tissue and implant parameters, source characteristics, and numerical inaccuracies—do not impact the general findings.

In conclusion, individuals with implants are at increased risk when in close proximity to WPT coils and other strong sources operating at frequencies < 450 MHz.

To protect the significant sub-population of persons with implants, safety standards should be revised, e.g., by lowering the reference levels or formulating procedures to ensure and demonstrate the safety of persons with implants, e.g., by evaluating typical implant trajectories. Similar precautions have already been successfully addressed for MRI exposures (ISO 2022).

Further studies should be undertaken to investigate more generic and standardizable approaches to the assessment of the safety of persons with implants exposed to WPT and other common and emerging frequencies, and more basic research could be directed towards understanding the threshold of nerve activation as a function of frequency to reduce the conservativeness of current reference levels.

Acknowledgments

The project (21NRM05 STASIS) has received funding from the European Partnership on Metrology, co-financed by the European Union's Horizon Europe Research and Innovation Program and by the Participating States. Open access publishing facilitated by The University of Western Australia, as part of the Wiley - The University of Western Australia agreement via the Council of Australian University Librarians.

Conflicts of Interest

The authors declare no conflicts of interest.

References

ASTM. *F2182 - 19e2: Standard Test Method for Measurement of Radio Frequency Induced Heating On or Near Passive Implants During Magnetic Resonance Imaging*, F2182-19e2, 2019. Accessed April 13, 2023. [Online]. Available: https://www.astm.org/f2182-19e02.html.

Fairfield Market Research., "Medical Implants Market—Global Industry Analysis, Size, Share, Growth, Trends, and Forecast 2031—By Product, Technology, Grade, Application, End-user, Region: (North

1521186x, 2025, 6, Downloaded from https://onlinelibrary.wiley.com/doi/10.1002/bem.70023, Wiley Online Library on [29/09/2025]. See the Terms and Conditions (https://onlinelibrary.wiley.com/terms-and-conditions) on Wiley Online Library for rules of use; OA articles are governed by the applicable Creative Commons License

America, Europe, Asia Pacific, Latin America and Middle East and Africa)," Fairfield Market Research, 5972660, May 2024. Accessed July 03, 2025. [Online]. Available: https://www.researchandmarkets.com/reports/5972660/medical-implants-market-global-industry.

Fortune Business Insights., "Wireless Charging Market Size, Share, Growth & Trends, 2032." Accessed July 02, 2025. [Online]. Available: https://www.fortunebusinessinsights.com/wireless-charging-market-105183.

Gosselin, M.-C., E. Neufeld, H. Moser, et al. 2014. "Development of a New Generation of High-Resolution Anatomical Models for Medical Device Evaluation: The Virtual Population 3.0." *Physics in Medicine and Biology* 59, no. 18: 5287–5303, September https://doi.org/10.1088/0031-9155/59/18/5287.

Hasgall, P. A., F. Di Gennaro, C. Baumgartner, et al. "IT'IS Database for Thermal and Electromagnetic Parameters of Biological Tissues, Version 4.1." Accessed July 04, 2025. [Online]. Available: https://itis.swiss/virtual-population/tissue-properties/database/dielectric-properties.

Henderson, J. M., J. Tkach, M. Phillips, K. Baker, F. G. Shellock, and A. R. Rezai. 2005. "Permanent Neurological Deficit Related to Magnetic Resonance Imaging in a Patient With Implanted Deep Brain Stimulation Electrodes for Parkinson's Disease: Case Report." *Neurosurgery* 57, no. 5: 1063, November https://doi.org/10.1227/01.NEU.0000180810.16964.3E.

Hirata, A., F. Ito, and I. Laakso. 2013. "Confirmation of Quasi-Static Approximation in SAR Evaluation for a Wireless Power Transfer System." *Physics in Medicine and Biology* 58, no. 17: N241, August https://doi.org/10.1088/0031-9155/58/17/N241.

IEC PAS., *IEC International Standard: Assessment Methods of the Human Exposure to Electric and Magnetic Fields From Wireless Power Transfer Systems - Models, Instrumentation, Measurement and Numerical Methods and Procedures (Frequency Range of 1 kHz to 30 MHz)*, 63184, 2021. Accessed July 04, 2025. [Online]. Available: https://webstore.iec.ch/en/publication/67745.

IEC/IEEE., "IEC/IEEE International Standard - Measurement procedure for the Assessment of Specific Absorption Rate of Human Exposure to Radio Frequency Fields From Hand-Held and Body-Mounted Wireless Communication Devices – Part 1528: Human Models, Instrumentation, and Procedures (Frequency range of 4 MHz to 10 GHz)," *IECIEEE 62209-15282020*, pp. 1–284, Oct. 2020, https://doi.org/10.1109/IEEESTD.2020.9231298.

IEC/IEEE., *IEC/IEEE International Standard: Determining the Peak Spatial-Average Specific Absorption Rate (SAR) in the Human Body From Wireless Communications Devices, 30 MHz to 6 GHz-part 1: General Requirements for Using the Finite-Difference Time-Domain (FDTD) Method for SAR Calculations*, 62704–1. Accessed July 04, 2025. [Online]. Available: https://webstore.iec.ch/en/publication/34411.

IEEE. 1992. "IEEE Standard for Safety Levels with Respect to Human Exposure to Radio Frequency Electromagnetic Fields, 3 kHz to 300 GHz." In *IEEE Std C951* (1991, 1–76, April. https://doi.org/10.1109/IEEESTD.1992.101091.

IEEE., "IEEE Standard for Safety Levels with Respect to Human Exposure to Radio Frequency Electromagnetic Fields, 3 kHz to 300 GHz," *IEEE Std C951-2005 Revis. IEEE Std C951-1991*, pp. 1–238, April 2006, https://doi.org/10.1109/IEEESTD.2006.99501.

IEEE., "IEEE Standard for Safety Levels with Respect to Human Exposure to Electric, Magnetic, and Electromagnetic Fields, 0 Hz to 300 GHz," *IEEE Std C951-2019 Revis. IEEE Std C951-2005 Inc. IEEE Std C951-2019Cor 1-2019*, pp. 1–312, October 2019, https://doi.org/10.1109/IEEESTD.2019.8859679.

International Commission on Non-Ionizing Radiation Protection (ICNIRP). 1998. "Guidelines for Limiting Exposure to Time-Varying Electric, Magnetic, and Electromagnetic Fields (Up to 300 GHz). International Commission on Non-Ionizing Radiation Protection." *Health Physics* 74, no. 4: 494–522, Apr.

International Commission on Non-Ionizing Radiation Protection (ICNIRP). 2010. "Guidelines for Limiting Exposure to Time-Varying Electric and Magnetic Fields (1 Hz to 100 KHz)." *Health Physics* 99, no. 6: 818–836, Dec. https://doi.org/10.1097/HP.0b013e3181f06c86.

International Commission on Non-Ionizing Radiation Protection (ICNIRP). 2020. "Guidelines for Limiting Exposure to Electromagnetic Fields (100 KHz to 300 GHz)." *Health Physics* 118, no. 5: 483–524, May. https://doi.org/10.1097/HP.0000000000001210.

ISO., *ISO/TS 10974: Assessment of the Safety of Magnetic Resonance Imaging for Patients With an Active Implantable Medical Device*, TS 10974, 2018. Accessed November 16, 2022. [Online]. Available: https://www.iso.org/cms/render/live/en/sites/isoorg/contents/data/standard/06/50/65055.html.

King, R. W. P., K. -M. Lee, S. R. Mishra, and G. S. Smith. 1974. "Insulated Linear Antenna: Theory and Experiment." *Journal of Applied Physics* 45, no. 4: 1688–1697, Apr. https://doi.org/10.1063/1.1663476.

King, R. W. P., B. Sandler, and T. T. Wu. 1969. "Cylindrical Antennas Immersed in Arbitrary Homogeneous Isotropic Media." *Journal of Applied Physics* 40, no. 13: 5049–5065, Dec. https://doi.org/10.1063/1.1657353.

Kyriakou, A., A. Christ, E. Neufeld, and N. Kuster. 2012. "Local Tissue Temperature Increase of a Generic Implant Compared to the Basic Restrictions Defined in Safety Guidelines." *Bioelectromagnetics* 33, no. 5: 366–374. https://doi.org/10.1002/bem.21695.

Laakso, I., "Computational Dosimetry at Low Frequencies: Recent Progress and Open Issues," in *2020 International Symposium on Electromagnetic Compatibility - EMC EUROPE*, September 2020, pp. 1–4. https://doi.org/10.1109/EMCEUROPE48519.2020.9245772.

Liorni, I., E. Neufeld, S. Kühn, et al. 2018. "Novel Mechanistic Model and Computational Approximation for Electromagnetic Safety Evaluations of Electrically Short Implants." *Physics in Medicine and Biology* 63, no. 22: 225015. https://doi.org/10.1088/1361-6560/aae94c.

Meier, K., "Scientific Bases for Dosimetric Assessments in Compliance Tests," Zurich, Switzerland, 1996.

Official Journal of the European Union., "Directive 2013/35/EU of the European Parliament and of the Council of 26 June 2013 on the Minimum Health and Safety Requirements Regarding the Exposure of Workers to the Risks Arising From Physical Agents (Electromagnetic Fields) (20th Individual Directive Within the Meaning of Article 16(1) of Directive 89/391/EEC) and Repealing Directive 2004/40/EC," 2013.

Park, S. W., K. Wake, and S. Watanabe. 2013. ""Calculation Errors of the Electric Field Induced in a Human Body Under Quasi-Static Approximation Conditions." *IEEE Transactions on Microwave Theory and Techniques* 61, no. 5: 2153–2160, May. https://doi.org/10.1109/TMTT.2013.2247211.

Qualcomm Technologies Inc., "Compliance Assessment of Human Exposure From Wireless Electric Vehicle Charging (wevc) System." 2014.

De Santis, V., M. Douglas, N. Kuster, and X. L. Chen, "Issues of ICNIRP Guidelines When Determining Compliance With LF Exposure Limits," in *International Symposium on Electromagnetic Compatibility - EMC EUROPE*, Septemeber 2012, pp. 1–4. https://doi.org/10.1109/EMCEurope.2012.6396800.

Schmid, G., P. Schneeweiss, R. Hirtl, T. Jhala, and T. Samaras. 2024. "Numerical Assessment of Induced Electric Fields in a Worker's Hand With Commonly Used Metallic Implants Under Exposure to Low Frequency Magnetic Fields." *Journal of Radiological Protection Official Journal of the Society for Radiological Protection* 44, no. 3: 1–17. August https://doi.org/10.1088/1361-6498/ad66dc.

1521186x, 2025, 6, Downloaded from https://onlinelibrary.wiley.com/doi/10.1002/bem.70023, Wiley Online Library on [29/09/2025]. See the Terms and Conditions (https://onlinelibrary.wiley.com/terms-and-conditions) on Wiley Online Library for rules of use; OA articles are governed by the applicable Creative Commons License

SPEAG., Schmid & Partner Engineering AG, "Verification and Validation (V&V) Sources for WPT." Accessed July 04, 2025. [Online]. Available: https://speag.swiss/components/emv-and-v-sources/wpt/.

ZMT Zurich MedTech AG., "SAIMD-U » zurich med tech." Accessed July 04, 2025. [Online]. Available: https://zmt.swiss/validation-hw/saimd/saimd-u/.

ZMT Zurich MedTech AG., "Sim4Life V8.0." Accessed July 03, 2025. [Online]. Available: https://zmt.swiss/news-and-events/news/sim4life/sim4life-v8-0-web-and-desktop-fully-compatible/.

1521186x, 2025, 6, Downloaded from https://onlinelibrary.wiley.com/doi/10.1002/bem.70023, Wiley Online Library on [29/09/2025]. See the Terms and Conditions (https://onlinelibrary.wiley.com/terms-and-conditions) on Wiley Online Library for rules of use; OA articles are governed by the applicable Creative Commons License